Chemical Engineering Journal 380 (2020) 122201

Contents lists available at ScienceDirect

Chemical Engineering Journal

journal homepage: www.elsevier.com/locate/cej

Sorbents screening for post-combustion CO_2 capture via combined temperature and pressure swing adsorption

Chaitanya Dhoke[a], Schalk Cloete[b], Shreenath Krishnamurthy[b], Hwimin Seo[c], Ignacio Luz[d], Mustapha Soukri[d], Yong-ki Park[c], Richard Blom[b], Shahriar Amini[a,b], Abdelghafour Zaabout[b,*]

[a] Norwegian University of Science and Technology, Trondheim, Norway
[b] Process Technology Department, SINTEF Industry, Trondheim, Norway
[c] Korea Research Institute of Chemical Technology, Daejeon, South Korea
[d] Engineering Systems, RTI International, Research Triangle Park, NC, USA

HIGHLIGHTS

- SARC, a novel reactor concept for low energy penalty adsorption-based CO_2 capture.
- The SARC concept employs heat and vacuum pumps for energy efficient sorbent regeneration.
- Polyethyleneimine sorbents were identified to be best suited for operation of SARC concept.
- Combination of high adsorption capacity and carbonation at low temperature minimizes the CO_2 capture penalty in SARC.

GRAPHICAL ABSTRACT

SARC working principle showing heat transfer from a reactor under carbonation to one under regeneration using a heat pump.

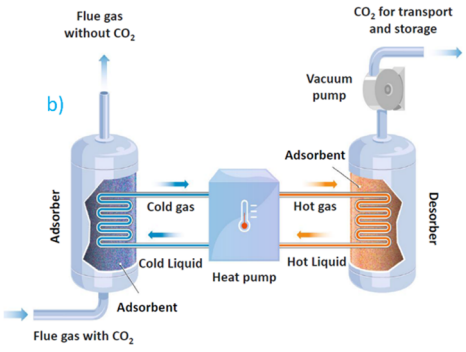

ARTICLE INFO

Keywords:
Adsorption
Post-combustion CO_2 capture
Polyethyleneimine
Sorbent screening
Swing adsorption fluidized bed reactor cluster

ABSTRACT

Adsorption-based post-combustion CO_2 capture is enjoying significant research attention due to its potential for significant reductions in energy penalty, cost and environmental impact. Recent sorbent development work has focussed on polyethyleneimine (PEI) and dry sorbents that exhibit attractively low regeneration energy requirements. The main objective of this study is to identify best suitable sorbent for the recently published swing adsorption reactor cluster (SARC) concept. The screening results of four sorbents indicated two PEI sorbents to be good candidates for SARC application: a PEI sorbent functionalized with 1,2-epoxybutane supported on silica (referred to as EB-PEI in the rest of the document) and a PEI sorbent supported on mesoporous silica containing confined metal organic framework nanocrystals (referred to as PEI-MOF in the rest of the document). High resolution single-component isotherms revealed substantial differences in adsorption capacity and optimal operating temperatures for the two PEI sorbents, and CO_2 and H_2O isotherm models were derived from this data. Subsequently, breakthrough experiments and lab-scale reactor tests showed that co-feeding of CO_2 and H_2O had no significant effect, allowing the single-component isotherm models to be safely used in large-scale reactor simulations. Such a reactor model was then employed to illustrate the effect of the sorbent adsorption char-

* Corresponding author at: Flow Technology Group, SINTEF Industry, S.P. Andersens vei 15 B, 7031 Trondheim, Norway.
E-mail address: abdelghafour.zaabout@sintef.no (A. Zaabout).

https://doi.org/10.1016/j.cej.2019.122201
Received 18 May 2019; Received in revised form 8 July 2019; Accepted 10 July 2019
Available online 11 July 2019

acteristics on the efficiency of the novel swing adsorption reactor cluster, which combines pressure and temperature swings. The EB-PEI and PEI-MOF sorbents were compared to a previously published PEI sorbent with distinctly different adsorption behaviour and recommendations for future sorbent development work were made.

List of symbols

SARC	swing adsorption reactor cluster
VPSA	vacuum pressure swing adsorption
VSA	vacuum swing adsorption
VTSA	vacuum combine temperature swing adsorption
TSA	temperature swing adsorption
PSA	pressure swing adsorption
ESA	electric thermal swing
CCUS	carbon dioxide capture, utilization and storage
COP	coefficient of performance
P&ID	process and instrumentation diagram
MFC	mass flow controller
LPM	liters/minutes
LHV	lower heating value
GJ	giga joules
t	tonne
MOF	metal organic framework
HP	heat pump
KRICT	Korea Research Institute of Chemical Technology, Daejeon, South Korea
RTI	Engineering Systems, RTI International, Research Triangle Park, NC, USA
WS	with water (H_2O)
WOS	without water (H_2O)
EB-PEI	1,2-epoxybutane functionalized polyethyleneimine supported on SiO_2 sorbent supplied by KRICT
PEI-MOF	polyethyleneimine and Metal organic framework supported on SiO_2 developed at RTI
K/ZrO_2	potassium sorbent supported on ZrO_2 (K/ZrO_2) supplied by KRICT
Na/ZrO_2	sodium sorbent supported on ZrO_2 (Na/ZrO_2) supplied by KRICT
SPECCA	specific primary energy consumption for CO_2 avoided ($MJ_{LHV}/kgCO_2$)
W_{HP}	heat pump power consumption
DCB	dynamic column breakthrough
q_{CO_2}	CO_2 loading on Sorbent
φ	relative humidity
E_{HP}	energy transfer by the heat pump
T_H	condensation temperatures of the heat pump working fluid
T_C	evaporation temperatures of the heat pump working fluid
p_{CO_2}	partial pressure of CO_2

1. Introduction

There is a growing interest in low temperature adsorption-based post combustion CO_2 capture due to its combined potential of reducing energy penalty and easy retrofitting with minimal integration with existing plants [1,2]. More importantly, this technology offers the flexibility of capturing CO_2 from different industrial CO_2 sources owing to its different sorbent regeneration modes (temperature/pressure swings) and reactor types, enabling different levels of integration with the plant, in addition to flexibility regarding the scale of the plant and its CO_2 partial pressure in the flue gas stream. Research in this field was largely dominated by sorbent development focussing on reducing the energy penalty mainly through minimizing the heat of reaction and maximizing the adsorption capacity, but also improving tolerance to impurities such as SOx and NOx [1,3]. Sorbents could be classified in two categories depending on the heat of CO_2 sorption; physisorption and chemisorption based, with specific advantages and drawbacks of each category [1,3], i.e. the former is more sensitive to pressure swing, being suitable to high CO_2 partial pressure gas streams, while the latter are more sensitive to temperature swing and can handle low CO_2 partial pressure gas streams. Recent research on physisorption focussed on MOF-based sorbents that possess high specific surface area, thus maximizing the absolute adsorption capacity [1,3–8]. As for the chemisorption-based sorbents, the largest focus is on the polyethyleneimine based (referred to as PEI in the rest of the document), given their relatively high adsorption capacity, good kinetics and insensitivity to water, thereby avoiding additional costly equipment for water removal and allowing greater process simplicity [1,3,9–11].

A suitable contacting system is a key factor for efficient utilization of each sorbent category, as it affects both the process efficiency, footprint and overall capture costs [3]. In other words, material development is tightly linked to the reactor configuration and regeneration mode [1,12]. To this end, different types of reactors were applied to adsorption-based CO_2 capture, including fixed [13,14], rotating [15], moving [16–18] and fluidized beds [19,20]. Substantial research has been conducted on the fixed bed, due to the simplicity of its basic design, testing hundreds of sorbents under different regeneration modes [13,14,21]. The vacuum swing regeneration mode proved to be the best against the temperature swing that resulted in very long cycle times due to the heat transfer limitation in heating and cooling in this reactor configuration [3,22]. A major drawback of this regeneration mode is the impracticality of drawing extreme vacuum at industrial scale for achieving the benchmark CO_2-purity requirement of 96%, dictating the use of a two-stage vacuum swing adsorption (VSA) system that increases costs and complexity [2,7,23]. A hybrid VSA CO_2 membrane system was proposed as an alternative to mitigate this fundamental challenge at acceptable process complexity [24]. Research trends on fixed bed shifted towards structured and monolithic reactors embedding high adsorption capacity sorbents and allowing high gas throughput with the ultimate aim of achieving cycles time below one minute in compact reactors [3,25–28].

As for fluidized and moving bed reactors, recent research on this configuration focusses on the use of multistage counter-current contactors that was shown to maximize the working adsorption capacity of the sorbent at smaller reactor heights and minimal solid circulation rate [29–31]. However, the main drawback is that the gas needs to be fed at small velocity to allow the solids to fall counter-current to the rising gas, resulting in large reactor footprint. Solids separation and circulation between the adsorber and desorber also introduces additional complexity. Another reactor configuration based on fluidized bed was proposed for heat integration between carbonation and regeneration, but using a heat pump [32]. This configuration, known as the swing adsorption reactor cluster (SARC), also uses a multistage fluidized bed to maximize the sorbent working adsorption capacity at acceptable reactor height, but operates under dense bed conditions using a cluster of reactors, each running a transient four-step cycle to capture CO_2. No solids circulation takes place between the reactors, allowing a vacuum swing to be deployed in parallel to the temperature swing. The vacuum swing minimizes the required temperature difference between carbonation and regeneration, thereby maximizing the heat pump efficiency

[32]. Thermodynamic assessments have shown that this concept can achieve energy penalties (quantified using the SPECCA parameter) as low as 2.59 $MJ_{LHV}/kgCO_2$ for a coal power plant [33] and 2.04 $MJ_{LHV}/kgCO_2$ for cement [34] for achieving 90% CO_2 capture and 96% CO_2 purity. The working principle of SARC is shown in Fig. 1 and a more detailed description of each step in the SARC cycle is given later in the reactor model description.

Fluidized bed reactors are preferred in SARC over the fixed beds normally used in dynamic processes implementing pressure swings in order to maximize the rate of heat transfer to the internal tubes carrying the heat pump working fluid. SARC reactors will operate with typical Geldart B particles and previous studies [32–34] have assumed a fluidization velocity of 1 m/s during the carbonation step, resulting in bubbling fluidization.

A polyetheleneimine sorbent was used in the simulation and tested in a small lab set up under SARC conditions as a first demonstration of the working principle [35]. This study further screens potential sorbents for identifying suitable ones for operation of the SARC concept. Four sorbents (two PEI-based, one potassium and one sodium based) were screened first in a 60 g reactor scale under real SARC conditions. Then isotherms were measured and fitted for the two best performing sorbents, which were subsequently used in SARC reactor simulations. The energetic performance of SARC with the two sorbents was evaluated using correlations for electricity consumption of the heat and vacuum pumps.

2. Methodology

2.1. Reactor tests

A lab scale experimental setup was built for demonstrating the working principle of SARC concept and for sorbents screening. A schematic illustration of this setup is shown in Fig. 2. The main components of the setup are a reactor body of 2 cm ID and 100 cm height, a heating jacket, a cooling water bath and a vacuum pump. It also had additional devices reactor monitoring and gas feed such as thermocouples, a pressure sensor, solenoid valves, mass flow controllers, etc. An online gas analyzer (ETG MCA 100 Syn Biogas Multigas Analyzer), sampling gases at the outlet of the atmospheric and vacuum vents, was used to measure the gas composition at 1 Hz frequency. The operation procedure of the experimental setup and additional details have already been published [35].

Experiments completed in this section were structured in two sets as summarized in Table 1, using four sorbents, two PEI-based; EB-PEI supplied by KRICT [36] and a PEI-MOF also supported on mesoporous silica containing confined metal organic framework nanocrystal [37,38] developed by RTI and two dry sorbents K/ZrO_2 and Na/ZrO_2 made by KRICT by spray-drying of the slurry that consists of 30 wt% alkali metal carbonate and 70% of ZrO_2. Other types of sorbents like activated carbon and zeolites were not considered because they typically have low regeneration enthalpies and therefore a low sensitivity to temperature swing. As discussed in a previous work [33], low regeneration enthalpies strongly increase the SARC energy penalty because a low temperature sensitivity requires a large temperature swing, which reduces the efficiency of the heat pump.

Each run of these experimental sets comprises of three steps: an adsorption step followed by a VTSA regeneration step and then a total regeneration step. All steps were long enough to ensure that equilibrium is reached. The last step of total regeneration was carried out by feeding 0.5 Nl/min of N_2 at 393–403 K for the PEI sorbents while, for K/ZrO_2 and Na/ZrO_2, it was carried out at higher temperatures, in the range of 463–546 K. The reason for regenerating the sorbent completely is to enable quantification of the adsorption capacity using Eq. (1) (the actual SARC concept will not include this last step of total regeneration).

The experimental sets were designed to investigate two main objectives. The first experimental set was designed to identify suitable sorbents with a high working capacity under SARC operating conditions. This was done by screening the sorbents at various levels of regeneration pressure and temperature swings. The gas composition was sampled continuously at the reactor outlet to estimate the adsorption and working capacity which is defined as follows:

$$Adsorption\ capacity = \frac{moles\ of\ CO_2\ adsorbed\ in\ carbonation}{kg\ of\ adsorbent} \quad (1)$$

$$Working\ capacity = \frac{moles\ of\ CO_2\ desorbed\ in\ VTSA\ step}{kg\ of\ adsorbent} \quad (2)$$

More specifically, the adsorption capacity is the maximum amount of CO_2 that can be adsorbed on the sorbent from a simulated flue gas stream with 12.5% CO_2. In order to quantify this using Eq. (1), the sorbent must be completely regenerated at the start of the carbonation step, hence the need for the total regeneration step mentioned earlier. On the other hand, the working capacity considers that the sorbent will not be fully regenerated by the VTSA in the SARC process. Specifically, the working capacity quantifies the maximum amount of additional CO_2 that can be adsorbed from the simulated flue gas on top of the CO_2 that remains on the sorbent after a VTSA regeneration step that is long enough to reach equilibrium.

The second experimental set was designed to study the effect of steam in the feed on the two PEI sorbents. To simulate real flue gas composition, a gas composition of 12.5% CO_2 and 87.5% N_2 (dry basis) was used for the carbonation. The effect of water vapor was studied by passing a mixed gas of CO_2 and N_2 through a temperature-controlled

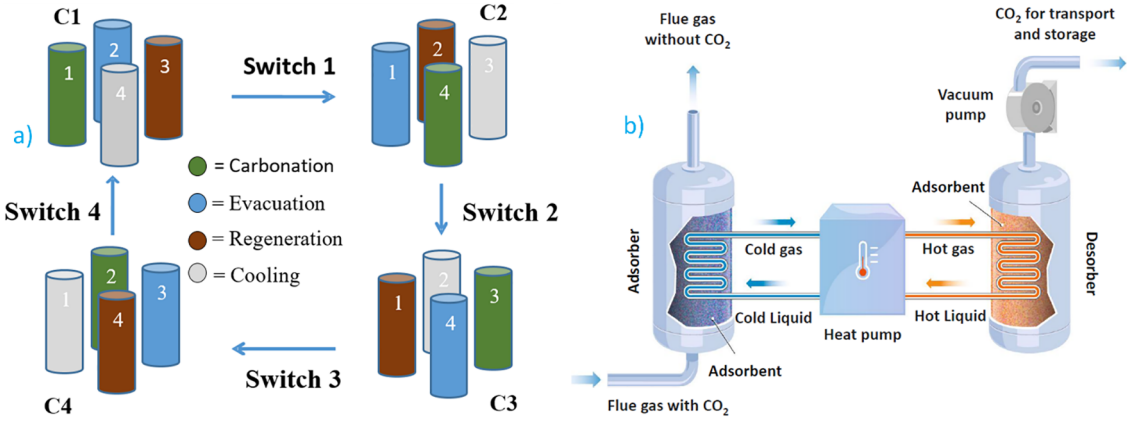

Fig. 1. SARC conceptual design: a) a cluster of SARC reactors for continuous gas stream processing; b) SARC working principle showing heat transfer from a reactor under carbonation to one under regeneration using a heat pump.

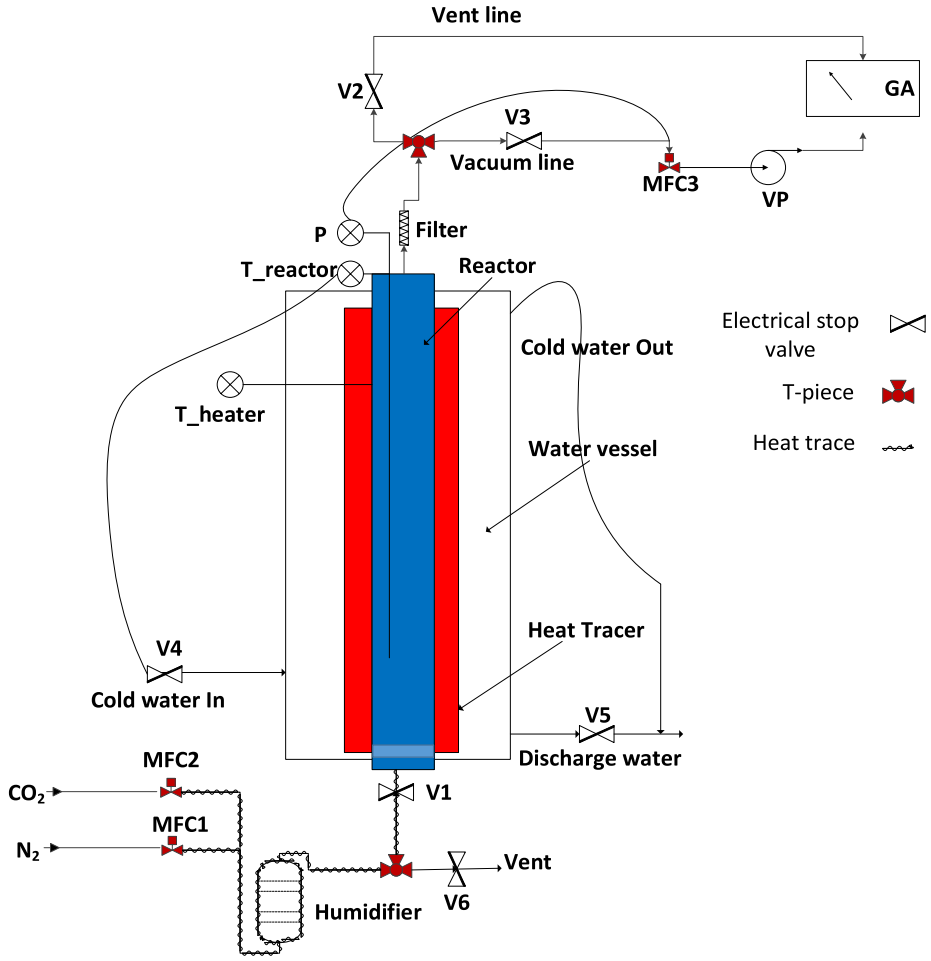

Symbols	Descriptions	Symbols	Descriptions
GA	Online gas analyzer	V1	Valve on feed inlet line to reactor
MFC1	Mass flowmeter for N_2	V2	Valve on atmospheric vent line
MFC2	Mass flowmeter for CO_2	V3	Valve on vacuum line
MF3	Mass flowmeter to control pressure inside reactor	V4	Valve on water inlet line
P	Pressure transmitter	V5	Valve on water discharge line
T_heater	Thermocouple measuring heater temperature (outside)	V6	Valve in humidifier outlet line
T_reactor	Thermocouple measuring adsorbent temperature (inside)	VP	Vacuum pump

Fig. 2. A P&ID of the experimental Setup for SARC cycle.

Table 1
Regeneration and carbonation conditions over the two experimental sets. All experiments were completed by conducting carbonation at atmospheric pressure in pressure of 12.5% CO_2 (dry basis) in N_2.

Experimental set	Objective	Sorbent	Adsorption temperature (K)	VTSA- regeneration		Steam addition (%)
				Temperature swing (K)	Regeneration pressure (kPa)	
1	Sorbents screening	EB-PEI	333 K	0–20 K	5–15 kPa	NA
		PEI-MOF	363 K	0–20 K	5–15 kPa	NA
		K/ZrO_2	353 K	20–60 K	5–15 kPa	6.5%
		Na/ZrO_2	333 K	20–60 K	5–15 kPa	6.5%
2	Effect of steam on 2 PEI sorbents	EB-PEI	333 K	20 K	10 kPa	5%
		PEI-MOF	363 K	20 K	10 kPa	5%

humidifier. The feed line was also heated to same temperature to avoid H_2O condensation. The concentration of H_2O was maintained by controlling the temperature of the humidifier and feed line. The content of water vapor in the simulated gas stream was calculated from the relative humidity and temperature measured at the inlet of the reactor.

For this campaign, the regeneration was carried in a VTSA step followed by total regeneration step as described earlier. The VTSA step was carried out by applying the temperature swing with vacuum as specified in Table 1, while the total regeneration step was conducted by purging 0.5 Nl/min of N_2 in the temperature range of 393–403 K without vacuum. In this experiment, the total regeneration step also served to ensure that no adsorbed water remains on the sorbent when transitioning from an experiment with steam addition to an experiment without steam addition.

2.2. Single component isotherms

Pure component CO_2 and H_2O isotherms were measured using a commercial volumetric apparatus from BEL inc. The volumetric apparatus has a reference cell which contains a known volume of gas and the sample cell which contains the sample. During experiments, gas flows from the reference cell to the sample cell and the amount adsorbed at equilibrium can be obtained from the difference in the pressure before and after adsorption in the reference cell.

78 mg of EB-PEI and 114 mg of PEI-MOF were packed in a sample cell and regenerated under vacuum overnight at 383 K. Once regeneration was complete, the samples were weighed again to record the dry weight and mounted on to the apparatus to proceed with the isotherm measurements. The isotherm measurement comprises of two steps: measurement of sample cell volume by helium followed by actual adsorption isotherm measurements.

For CO_2 the adsorption isotherms were measured from 333 to 403 K in 10 K increments from 0.1 kPa to 100 kPa. In case of H_2O the maximum temperature was set to 373 K and the isotherms were measured up to 4 kPa due to limitations of the instrument. In this study, the final dry weights of the EB-PEI and PEI-MOF samples were 71 mg and 106 mg respectively.

2.3. Breakthrough experiments

The two samples were further characterized by dynamic column breakthrough (DCB) experiments. In this setup, a known mass of the sample is saturated with the adsorbate (CO_2/H_2O) in a carrier gas, nitrogen. The adsorbed gas was then desorbed by switching the flow to the pure carrier gas. The exit concentration profile is continuously monitored by the detector. The information on adsorption equilibrium can be obtained by performing a mass balance on the concentration response curve.

The breakthrough set-up used in this study is shown in Fig. 3. It consists of an adsorption column housed inside an oven. The length and diameter of the adsorption column are 12 cm and 0.77 cm respectively. The flow rates of CO_2 and N_2 were controlled by mass flow controllers and water vapour was introduced by bubbling the CO_2 and N_2 mixture through a saturator. About 2 g of the sample was packed in the column and regenerated overnight at 383 K under a helium purge before each experiment. The breakthrough apparatus was used to study the adsorption equilibrium under dry and wet conditions with N_2 gas as a carrier. Two gas compositions were studied: 1) 22% CO_2 and 78% N_2 and 2) 22% CO_2, 2% H_2O and 76% N_2.

2.4. Reactor simulations

This study employs the reactor model developed for the swing adsorption reactor cluster (SARC) in an earlier work [32]. A single SARC reactor is modelled as four continuously stirred tank reactors (CSTRs) in series using MATLAB. This assumption ensures that the behaviour of the SARC reactor falls between that of a complete CSTR and a complete plug flow reactor (PFR), as would be the case in a fluidized bed with many internal obstructions to limit back-mixing. As shown in Zaabout, Romano [32], a greater number of CSTRs in series shifts the model behaviour increasingly towards that of a PFR, leading to better CO_2 capture rates. However, it was argued that four CSTRs in series represents a good compromise between CO_2 capture performance and practicality. Future experimental work will be required to better quantify the degree to which back-mixing can be restricted in a single-stage SARC reactor to achieve PFR-like behaviour, particularly whether the heat transfer tubes in the reactor are sufficient or whether additional flow obstructions are required.

The transient reactor model simulates the four steps in the SARC cycle as graphically illustrated in Fig. 4:

1. Carbonation: The flue gas is fed at close to atmospheric pressure to a regenerated sorbent bed and most of the CO_2 is adsorbed. The heat

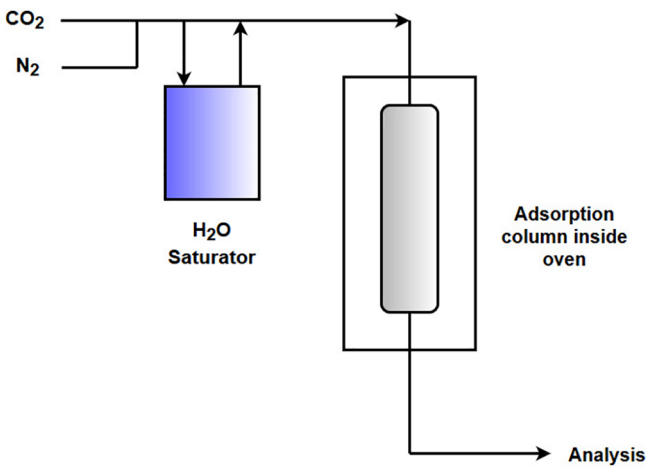

Fig. 3. Schematic drawing of the breakthrough set-up.

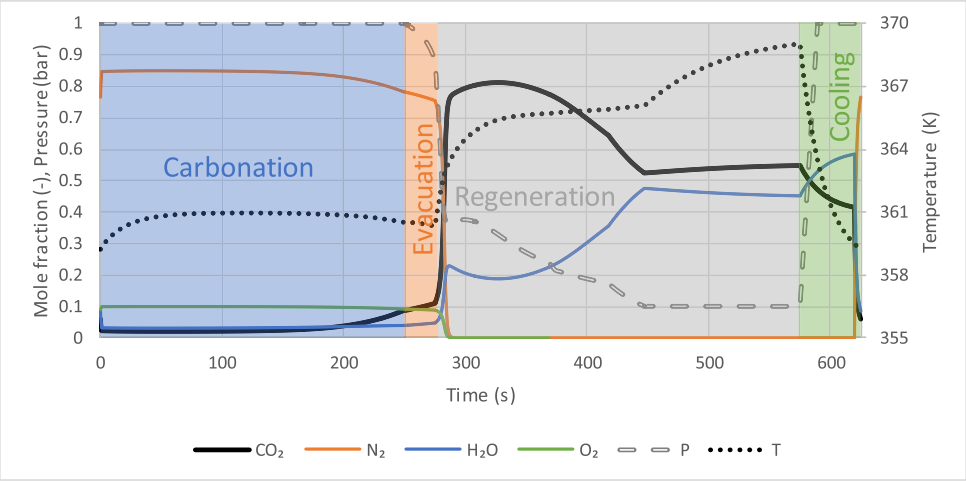

Fig. 4. Typical transient cycle of the SARC reactor.

pump continuously extracts the heat from the exothermic carbonation reaction to keep the reactor temperature close to constant.

2. Evacuation: In this short step, the evacuation pump extracts a portion of the N_2-rich gases in the reactor and vents these gases to the atmosphere to ensure a sufficiently high CO_2 purity from the subsequent regeneration step. No gas is fed to the reactor in this step.
3. Regeneration: The main vacuum pump draws a strong vacuum while the heat pump continuously adds heat into the reactor. The resulting combined pressure and temperature swing causes the sorbent to release CO_2, which is extracted by the vacuum pump and sent to the downstream CO_2 compression train. The CO_2 release may be enough to fluidize the bed, but prior process simulations have assumed that 10% of the extracted CO_2 is recycled to ensure good fluidization (see Fig. 3 in Cloete, Giuffrida [34]).
4. Cooling: Before the next carbonation step, the reactor must be cooled by the heat pump to ensure a sufficiently high CO_2 capture ratio at the start of the subsequent carbonation step. Flue gas is fed at 10% of the fluidization velocity used in the carbonation step.

Since the evacuation and cooling steps require much less time than the carbonation and regeneration steps, a large cluster of 25 reactors is required to achieve a steady state process unit [34]. The SARC reactor model repeats this transient cycle of four steps multiple times, each time adjusting the condensation temperature of the heat pump (to achieve 90% CO_2 capture by changing the amount of temperature swing) and the evacuation pump extraction rate (to achieve 96% CO_2 purity by changing the amount of N_2-rich gases extracted in the evacuation step). The final model result is taken only for the final cycle where the objective of 90% CO_2 capture and 96% CO_2 purity is met.

SARC consumes only electrical power, making it attractive for retrofit applications. Four main sources of power consumption are present: CO_2 compression, the vacuum pumps (a large pump for the regeneration step and a small pump for the evacuation step), the heat pump and the flue gas blower required to feed the flue gas through the reactors. This study will focus only on the consumption of the heat pump and main vacuum pump, which will be influenced by the sorbent isotherm. The remaining sources of power consumption will remain constant if the reactor size, flue gas flowrate and regeneration pressure are kept constant.

Heat pump power consumption will be estimated using Eq. (3), where W_{HP} is the heat pump power consumption, E_{HP} is the energy transfer by the heat pump from carbonation to regeneration, $C = 0.72$ is the fraction of theoretical maximum efficiency achieved in [34], and T_H and T_C are the hot (condensation) and cold (evaporation) temperatures of the heat pump working fluid.

$$\frac{E_{HP}}{W_{HP}} = C\frac{T_H}{T_H - T_C} \tag{3}$$

Vacuum pump power consumption will be scaled proportionately to the gas volume flowrate being extracted through the vacuum pump

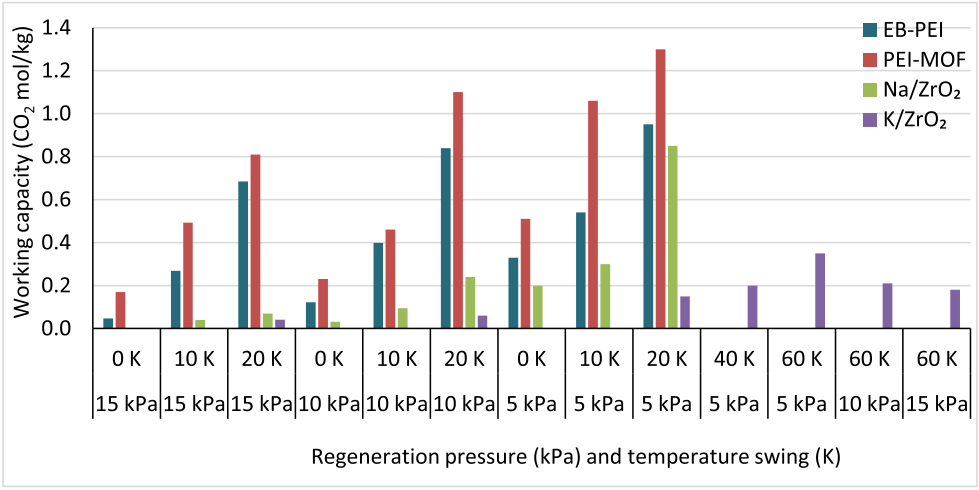

Fig. 5. Working capacity for four sorbents under different combinations of temperature and vacuum swing.

relative to a gas volume flowrate of 236 m^3/s for a power consumption of 6.44 MW for the central case (0.1 bar vacuum) in [34]. All other aspects of the simulation are kept constant to the aforementioned study to facilitate a direct investigation into the effect of the change in the isotherm on the SARC reactor performance.

3. Results and discussion

Results will be presented and discussed in four sections. First, the adsorbent screening and effect of higher H_2O concentrations will be investigated in a lab-scale reactor. Next, the single component isotherms for CO_2 and H_2O will be presented for the two-best performing sorbents together with the associated model fits. Subsequently, the effect of simultaneous CO_2 and H_2O adsorption will be studied in breakthrough experiments. And finally, the performance of the two sorbent isotherms presented in this work will be evaluated in large-scale reactor simulations for the swing adsorption reactor cluster (SARC) concept.

3.1. Reactor experiments

The working capacity (quantified in VTSA step) measured experimentally for four sorbents is presented in Fig. 5 for various VTSA process conditions. As expected, the working capacity increases with increasing vacuum level and regeneration temperature. Overall, PEI sorbents (EB-PEI and PEI-MOF) indicate better working capacity under VTSA operation as compared to dry sorbents (K/ZrO_2 and Na/ZrO_2). Na/ZrO_2 performed reasonably well at the strongest vacuum (5 kPa), but such vacuums may not be practically achievable in large scale SARC applications.

In general, PEI sorbents work well with a small temperature swing as compared to dry sorbents. This small temperature swing (20 K) is an important parameter in SARC concept as it improves the COP of the heat pump. Between the two PEI sorbents tested, PEI-MOF achieved the highest working capacity which is 37% more than EB-PEI working capacity. Within the ranges investigated in this study, the temperature has a larger effect than the vacuum pressure.

The effect of water was studied on best performing PEI sorbents. The adsorption capacity with H_2O present in the feed (5%) and without H_2O is presented in the Fig. 6. The variability in measured adsorption capacity in the experiments is indicated by the standard deviation bars. The adsorption capacity from single component isotherm models (presented later in Eqs. (4)–(7) and Table 1) for both PEI sorbents is also plotted for comparison. As seen in the Fig. 6, the experimental adsorption capacity for both sorbents is close to the respective single isotherm model predictions. It was interesting to observe that, even at higher H_2O (5%) concentration, the adsorption capacity remains unchanged for both the sorbents. As predicted from single component isotherm, PEI-MOF achieves 40% more adsorption capacity as compared to EB-PEI in lab scale experiments.

The working capacity (Eq. (2)) at 10 kPa and 20 K of temperature swing is presented in Fig. 7 for two PEI sorbents with and without H_2O. It was interesting to see the increase in the working capacity by the addition of the H_2O for both PEI sorbents. This increase could be related to the dilution of CO_2 because of simultaneous desorption of water. The resulting reduced CO_2 partial pressure increases the driving force for regeneration, which improves the working capacity for both the PEI sorbents.

Another perspective is given by plotting the working capacity with H_2O for both PEI sorbents at 10 kPa next to the working capacity at 5 kPa mbar and temperature swing of 20 K without H_2O in Fig. 8. Interestingly, the working capacity with H_2O at 10 kPa comes close to the case at 5 kPa without H_2O. As discussed in an earlier work [33], this added partial pressure swing facilitated by the release of H_2O during regeneration cancels out the energy penalty of additional heat supply required to release the H_2O and the added gas volume that must be extracted through the vacuum pump. Co-adsorption of H_2O and CO_2 from the flue gas is therefore not a problem for the SARC concept, although it will increase the energy penalty of pure TSA adsorption processes.

3.2. Isotherm fits

Experimentally determined CO_2 isotherms for the two well-performing PEI sorbents are presented in Fig. 9. Two key differences are observed between the two sorbents: 1) The adsorption capacity of PEI-MOF is about 40% higher than EB-PEI and 2) PEI-MOF appears to be qualitatively similar to EB-PEI at about 30 K higher temperatures.

The isotherms in Fig. 9 were described using the Toth model because a more simplified Langmiur isotherm model could not capture the shape of the isotherms with sufficient accuracy. Eqs. (4)–(7) give the general form of the Toth isotherm and Table 2 lists the different model coefficients of the fit for each sorbent. The sorbent loading (q_{CO_2}) is expressed in mol/kg as a function of the CO_2 partial pressure (p_{CO_2}) in kPa and the temperature (T) in K.

$$q_{CO_2} = \frac{n_s b p_{CO_2}}{(1 - (b p_{CO_2})^t)^{\frac{1}{t}}} \tag{4}$$

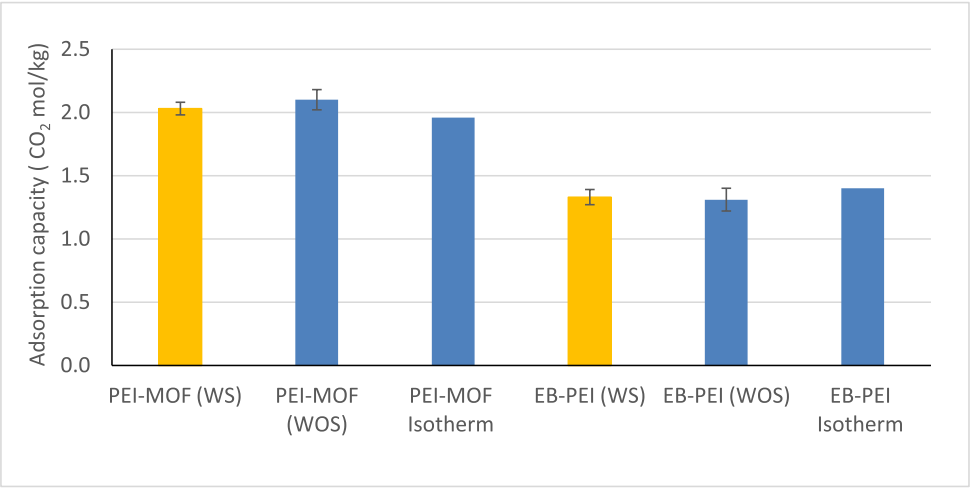

Fig. 6. Adsorption capacity for two PEI sorbents, with and without H_2O; *WOS – Without H_2O; *WS – with 5% H_2O.

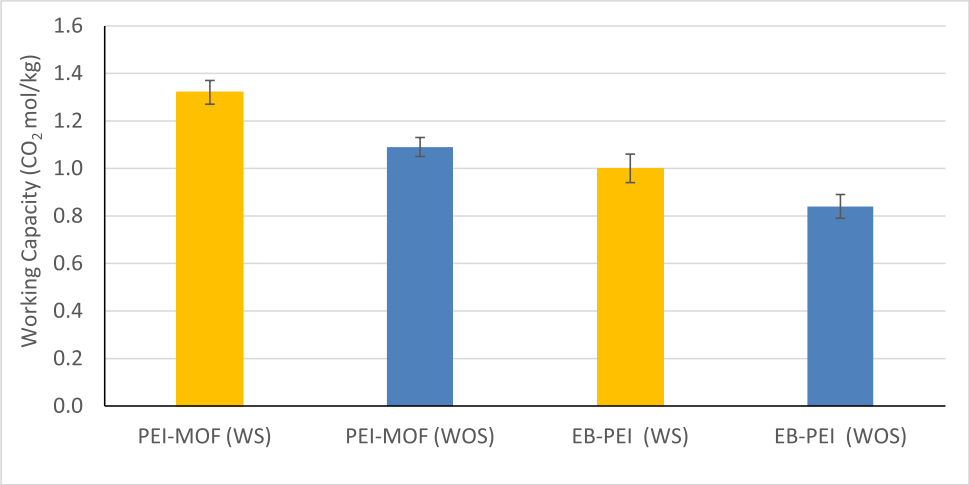

Fig. 7. Effect of H_2O on the working capacity of two PEI sorbents; *WS – With 5% H_2O; *WOS – Without H_2O.

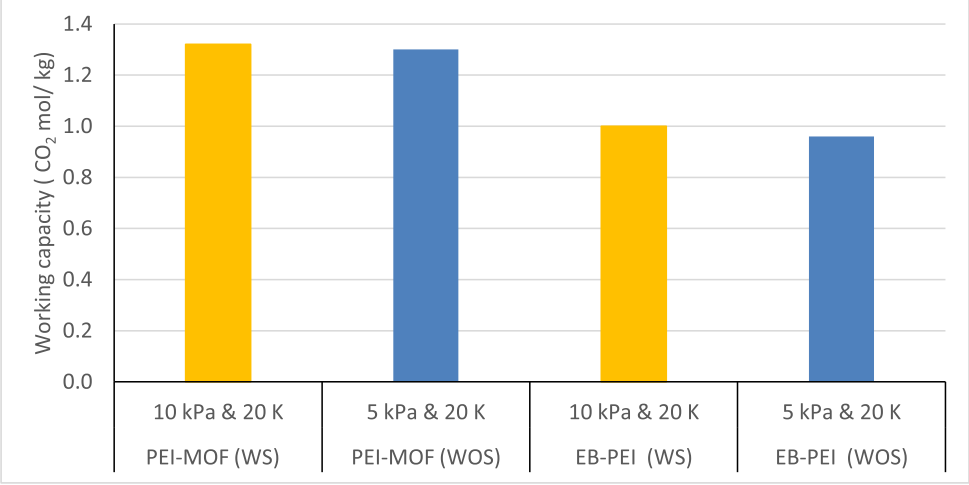

Fig. 8. Working capacity for two PEI sorbents at 10 kPa with steam and 5 kPa without steam; *WS – With 5% H_2O; *WOS – Without H_2O.

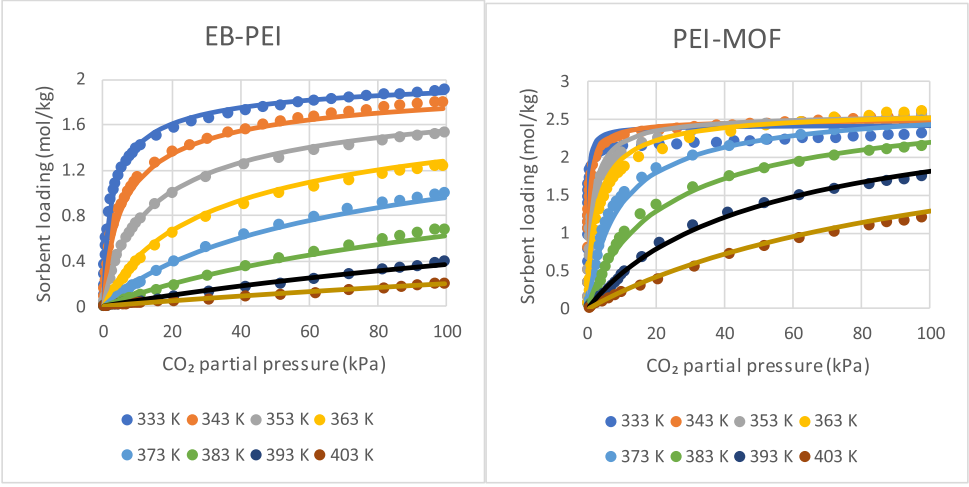

Fig. 9. Experimental CO_2 adsorption isotherms (symbols) and model fits (lines) for the two PEI sorbents.

Table 2
Model coefficients for use in Eqs. (4)–(7) to yield the fit illustrated in Fig. 9.

Coefficient	EB-PEI	PEI-MOF
$n_{s,0}$	2.146	2.200
X	0.317	−0.983
b_0	38.25	657.6
dH	104,581	113,958
t_0	0.497	0.710
α	1.273	0.714
T_0	303	303

$$n_s = n_{s,0}\exp\left(X\left(1-\frac{T}{T_0}\right)\right) \quad (5)$$

$$b = b_0\exp\left(\frac{dH}{RT_0}\left(\frac{T_0}{T}-1\right)\right) \quad (6)$$

$$t = t_0 + \alpha\left(1-\frac{T_0}{T}\right) \quad (7)$$

Subsequently, the H_2O isotherms were experimentally measured, and model fits were determined as illustrated in Fig. 10. All the data showed a simple linear relationship with the relative humidity, φ. The resulting model is described by Eq. (8) for EB-PEI and Eq. (9) for PEI-MOF.

$$q_{H_2O,EB\text{-}PEI} = \begin{cases} 5.69\varphi + 0.2528 \\ 37.66\varphi \text{ if } \varphi < 0.0087 \end{cases} \quad (8)$$

$$q_{H_2O,PEI\text{-}MOF} = \begin{cases} 13.33\varphi + 0.2416 \\ 35.48\varphi \text{ if } \varphi < 0.0109 \end{cases} \quad (9)$$

3.3. Breakthrough experiments

The breakthrough profile of CO_2 for EB-PEI is shown in Fig. 11. After regeneration, the column was kept under nitrogen flow until the experimental temperature was attained. The sample was then saturated 22% CO_2 in nitrogen followed by desorption using pure N_2. As seen from the profile, the adsorption profile was sharper. The breakthrough time was 1 min. In case of the desorption, the response was more spread and this was used to obtain the equilibrium information. To account for the dead volume in the system, a similar breakthrough procedure was carried out with an empty column. In both the cases the total flowrates in the adsorption and desorption were 120 and 50 ml/min respectively.

The adsorption equilibrium at 22 kPa, 13 kPa and 7.5 kPa were

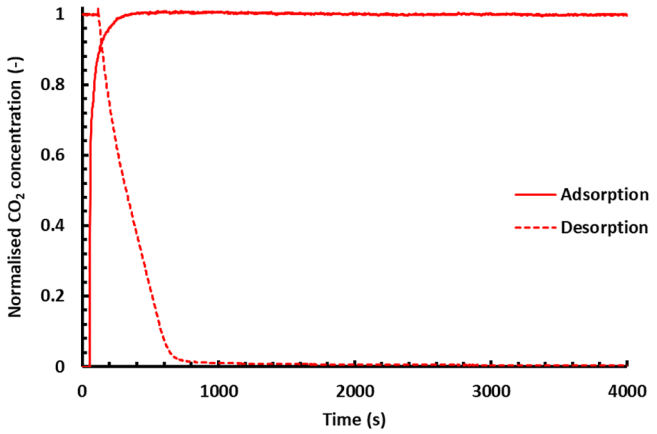

Fig. 11. Adsorption-Desorption profiles for CO_2 breakthrough in EB-PEI. The feed concentration was 22% CO_2 and 78%

obtained by subtracting the empty column desorption response from the packed column desorption response at the same concentrations (shown in Fig. 9) by doing the following mass balance around the column:

$$q^* = \frac{FC_T}{m_{ads}}\left(\int_o^t \frac{\frac{c(t)}{c_0}}{1-\frac{c(t)}{c_0}y0}\bigg|_{packed} - \int_o^t \frac{\frac{c(t)}{c_0}}{1-\frac{c(t)}{c_0}y0}\bigg|_{blank}\right)$$

where F is the total carrier flowrate during desorption, C_T is the total gas phase concentration, and m_{ads} is the mass of adsorbent. The denominator in the integral is the flow rate correction during desorption.

As the feed concentration is 22% CO_2, integrating the curves from $C/C_0 = 1$ from the base line would give the capacity at 22 kPa, while integrating from 0.59 and 0.34 to the baseline will give the capacity at 13 and 7.5 kPa respectively. The isotherms from the breakthrough are compared with the corresponding temperatures at the volumetry (presented in the previous section). In general, there is a good agreement between the two systems as shown in Fig. 12.

Experiments were also carried out with 2% water in both the samples. As seen from Fig. 12, no change took place when adding H_2O, indicating that both sorbents are tolerant to moisture.

3.4. Reactor simulations

Reactor simulations were completed at different carbonation temperatures for three PEI sorbents: the Veneman sorbent presented in [9]

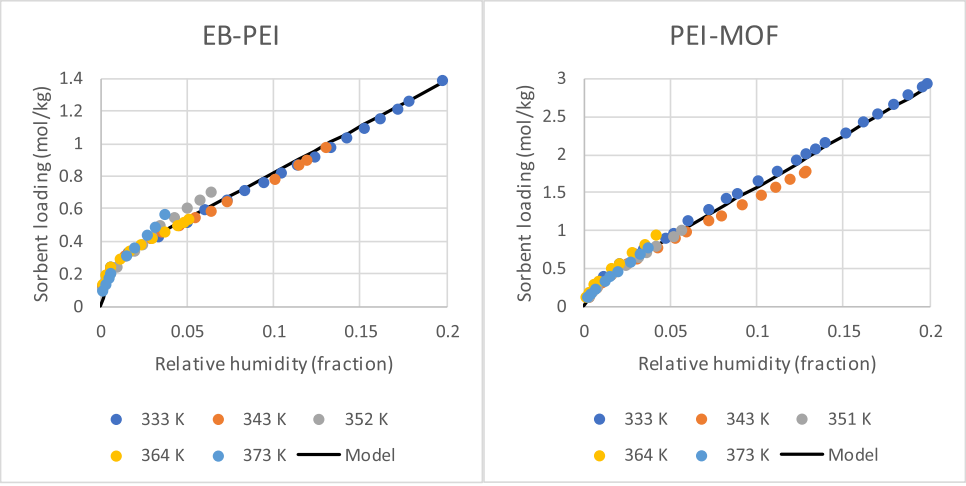

Fig. 10. Experimental H_2O adsorption isotherms (symbols) and model fits (lines) for the two PEI sorbents.

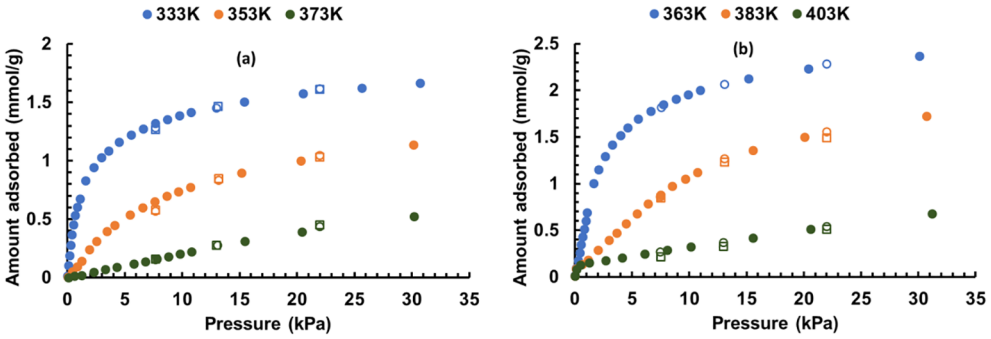

Fig. 12. CO_2 isotherms in (a) EB-PEI and (b) PEI-MOF. Solid symbols denote volumetric experiments, while open circles and squares denote dry and wet breakthrough experiments with 2% H_2O respectively.

used previously to model the SARC performance in a coal [32] and a cement plant [34] and the two sorbents investigated in this study. Changing the carbonation temperature (the flue gas inlet temperature is set equal to the carbonation temperature) will change average sorbent loading during the SARC cycle, with higher temperatures generally keeping the sorbent in a less carbonated state.

The combined heat and vacuum pump consumptions of the three sorbents at different carbonation temperatures are illustrated in Fig. 13, showing a clear optimum for each sorbent. As could be anticipated from the preceding results, PEI-MOF exhibits better working adsorption capacity at temperatures 30 K higher than EB-PEI. From an efficiency point of view, this results in a lower heat pump power consumption (because of a higher T_H in Eq. (3), but a higher vacuum pump power consumption (because of a larger gas volume at higher temperatures). In this case, the negative effect on the vacuum pump consumption outweighs the positive effect on the heat pump consumption, making the total power consumption of PEI-MOF higher than EB-PEI.

The good performance of EB-PEI is surprising in this case because it has a substantially smaller maximum CO_2 adsorption capacity than the other two sorbents. A higher CO_2 adsorption capacity is positive for SARC energy efficiency because it allows for more CO_2 to be adsorbed in each SARC cycle where the sorbent needs to be heated and cooled. The sensible heat transfer needed to heat and cool the sorbent therefore yields more CO_2. In this case, this effect is relatively small because of the small temperature swing (about 8 K) and the resulting high efficiency of the heat pump, thus reducing the importance of a high CO_2 adsorption capacity.

Fig. 13b shows the effect of carbonation time on each sorbent. Longer carbonation times will increase the amount of CO_2 adsorbed in each cycle, requiring a larger temperature swing, which will decrease the heat pump efficiency. On the other hand, the total amount of sensible heat required per unit of CO_2 captured in each cycle will reduce with longer carbonation times, countering the lower heat pump efficiency. Clearly, an optimum is also reached for each sorbent where the trade-off between these two conflicting effects is minimized.

As expected, PEI-MOF performs best a longer carbonation times where its higher adsorption capacity is well utilized. EB-PEI operates best at shorter carbonation times because its lower CO_2 adsorption capacity cannot facilitate as much CO_2 uptake in each cycle. Even so, the optimal power consumption with the EB-PEI sorbent remains lower than that of the PEI-MOF sorbent. This is due to the higher vacuum pump consumption required to extract the hotter gases from the PEI-MOF sorbent. If the PEI-MOF sorbent could operate optimally at a 30 K lower carbonation temperature like the EB-PEI sorbent, it would have had the lowest total power consumption. It should be noted, however, that the longer optimal cycle time of the PEI-MOF sorbent will be beneficial in reducing the frequency of switching of the reactor inlet and outlet valves as well as the valves directing the heat pump working fluid between the different reactors. This will increase valve lifetime and, if there is a significant time delay involved in switching, it can improve the overall process throughput rate.

Interestingly, the Veneman sorbent also operates best at relatively low carbonation times, despite having the highest CO_2 adsorption capacity of all the sorbents (~3 mol/kg). As shown in Fig. 14, this is due to the Veneman sorbent having a distinctly different isotherm shape and a lower temperature sensitivity, making less of its high CO_2 adsorption capacity accessible via reasonable temperature and pressure swings. This distinction between absolute CO_2 adsorption capacity and practically accessible CO_2 adsorption capacity is important for judging the attractiveness of different CO_2 capture sorbents.

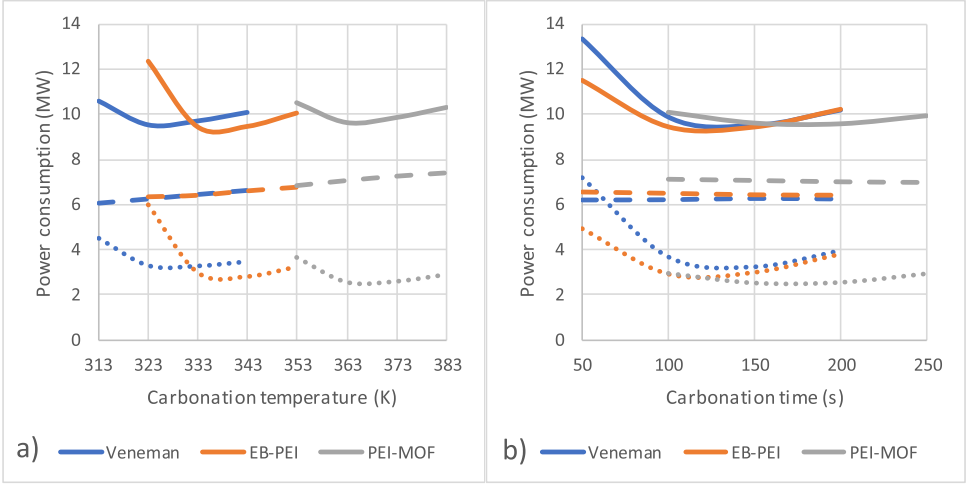

Fig. 13. Heat pump (dotted lines) and vacuum pump (dashed lines) power consumptions for the three sorbents: a) the effect of carbonation temperature at a carbonation time of 150 s and b) the effect of carbonation time at the optimal carbonation temperature of each sorbent. The solid line indicates the combined heat and vacuum pump power consumption.

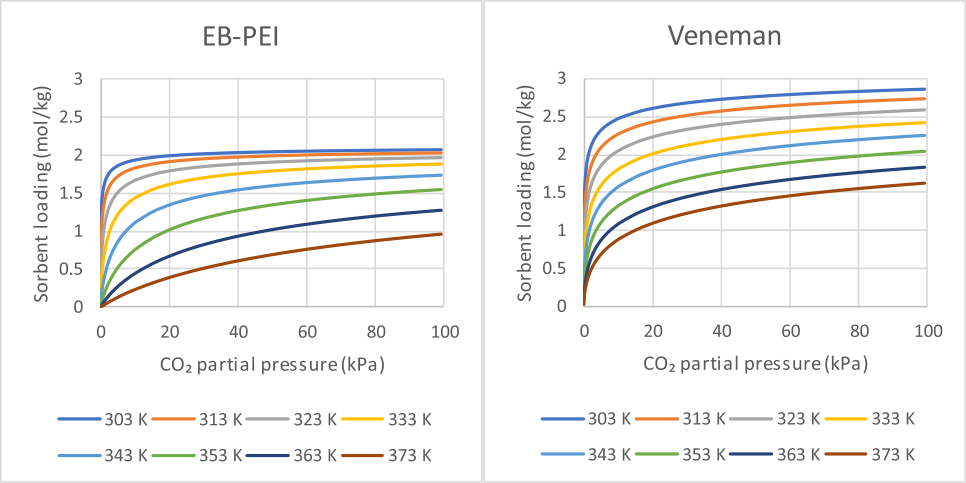

Fig. 14. Comparison between the CO_2 adsorption isotherms of EB-PEI sorbent from the current study (Table 2) and the sorbent presented by Veneman et al. [9]

4. Summary and conclusions

This work has evaluated the performance of two new polyethyleneimine (EB-PEI and PEI-MOF) sorbents and two dry sorbents (K/ZrO_2 and Na/ZrO_2) for application in the SARC concept. Their performance was evaluated by performing lab scale experiments in a fluidized bed reactor, where the two PEI sorbents (EB-PEI and PEI-MOF) clearly showed the best performance under SARC operating conditions.

High resolution single-component isotherms for CO_2 and H_2O adsorption by both PEI sorbents showed that the PEI-MOF has a substantially higher CO_2 and H_2O adsorption capacity than EB-PEI. In addition, the optimal operating temperature for PEI-MOF appears to be around 30 K higher than that of EB-PEI. This has important implications for the application of the sorbents in SARC concept. For example, EB-PEI operates best at a carbonation temperature around 333 K, which is a typical coal power plant flue gas exhaust temperature. Operating PEI-MOF at 363 K instead will reduce the amount of heat recovery from the flue gas stream, leading to some efficiency penalty. Higher temperature flue gases are common in some industrial processes where complete heat recovery is of lesser importance. Such processes, such as cement production, can be more suitable to PEI-MOF.

Breakthrough experiments showed no interaction effects of co-feeding CO_2 and H_2O, leading to the conclusion that the single-component isotherms can safely be used in reactor modelling studies using these sorbents. This result was confirmed via experiments conducted in a lab-scale reactor running the swing adsorption reactor cluster (SARC) cycle. The behaviour of this lab-scale reactor could be accurately predicted using the single component isotherms derived in this study, adding further confidence in reactor modelling studies based on easily derived single-component isotherms.

Finally, large scale reactor simulations using these two sorbents illustrated the effect of the difference in the isotherms on the energy efficiency of the SARC process. PEI-MOF, operating at a higher temperature, achieved lower heat pump power consumption, but also imposed a higher vacuum pump power consumption. Its higher adsorption capacity allowed for optimal operation at longer cycle times, which will reduce the wear on the valves in the SARC process. However, the substantially higher adsorption capacity of PEI-MOF did not result in an efficiency advantage relative to EB-PEI, mainly due to the higher vacuum pump power consumption.

The CO_2 adsorption isotherms of EB-PEI and PEI-MOF were qualitatively similar and were compared via simulation to a published PEI sorbent used in earlier SARC modelling works. The CO_2 adsorption isotherm of this sorbent showed clear qualitative differences compared to the sorbents investigated in the present work, making a significant portion of its high CO_2 adsorption capacity inaccessible via practically achievable pressure and temperature swings.

In summary, significant differences were observed between two different PEI sorbents developed by different research groups. Generally, it is beneficial to maximize the sorbent working capacity, lower the optimal operating temperature and achieve a CO_2 adsorption isotherm that allows for high degrees of regeneration at practically achievable CO_2 partial pressures. None of the sorbents investigated in this study achieved all three of these criteria, leaving room for future optimization of PEI sorbents for CO_2 capture using the SARC concept.

Acknowledgement

This study was performed as part of the project entitled “Demonstration of the Swing Adsorption Reactor Cluster (SARC) for simple and cost-effective post-combustion CO2 capture”, funded by the Research Council of Norway under the CLIMIT program (grant no. 268507/E20). The assistance of technical staff at the VATL lab (Reidar Tellebon, Inge Håvard Rekstad and Morten Grønli) in constructing and maintaining the lab scale reactor is greatly appreciated. We also thank Aud Bouzga for running few of the isotherms.

References

[1] A. Samanta, et al., Post-combustion CO2 capture using solid sorbents: a review, Indus. Eng. Chem. Res. 51 (4) (2012) 1438–1463.
[2] P.A. Webley, Adsorption technology for CO2 separation and capture: a perspective, Adsorption 20 (2–3) (2014) 225–231.
[3] J.C. Abanades, et al., Emerging CO2 capture systems, Int. J. Greenhouse Gas Control (2015).
[4] F. Rezaei, et al., Comparison of traditional and structured adsorbents for CO2 separation by vacuum-swing adsorption, Indus. Eng. Chem. Res. 49 (10) (2010) 4832–4841.
[5] A. Andersen, On the development of Vacuum Swing adsorption (VSA) technology for post-combustion CO2 capture, in: T. Dixon, K. Yamaji (Eds.), Ghgt-11, 2013, pp. 33–39.
[6] F. Brandani, et al., Adsorption kinetics and dynamic behavior of a carbon monolith, Adsorption 10 (2) (2004) 99–109.
[7] C. Shen, et al., Two-stage VPSA process for CO2 capture from flue gas using activated carbon beads, Indus. Eng. Chem. Res. 51 (13) (2012) 5011–5021.
[8] L. Wang, et al., CO2 capture from flue gas by two successive VPSA units using 13XAPG, Adsorption 18 (5–6) (2012) 445–459.
[9] R. Veneman, et al., Adsorption of H2O and CO2 on supported amine sorbents, Int. J. Greenhouse Gas Control 41 (2015) 268–275.
[10] T.O. Nelson, et al., RTI's solid sorbent-based CO2 capture process: technical and economic lessons learned for application in coal-fired, NGCC, and cement plants, Energy Procedia 114 (2017) 2506–2524.
[11] Y.C. Park, et al., Demonstration of pilot scale carbon dioxide capture system using dry regenerable sorbents to the real coal-fired power plant in Korea, Energy Procedia 4 (2011) 1508–1512.
[12] M. Bui, et al., Carbon capture and storage (CCS): the way forward, Energy Environ. Sci. 11 (5) (2018) 1062–1176.

[13] P.A. Webley, J. Zhang, Microwave assisted vacuum regeneration for CO2 capture from wet flue gas, Adsorption 20 (1) (2014) 201–210.
[14] M. Luberti, G.D. Oreggioni, H. Ahn, Design of a rapid vacuum pressure swing adsorption (RVPSA) process for post-combustion CO2 capture from a biomass-fuelled CHP plant, J. Environ. Chem. Eng. 5 (4) (2017) 3973–3982.
[15] T. Gupta, R. Ghosh, Rotating bed adsorber system for carbon dioxide capture from flue gas, Int. J. Greenhouse Gas Control 32 (2015) 172–188.
[16] C.A. Grande, et al., Development of moving bed temperature swing adsorption (MBTSA) process for post-combustion CO2 capture: initial benchmarking in a NGCC context, Energy Procedia 114 (2017) 2203–2210.
[17] T. Okumura, et al., CO2 capture test for a moving-bed system utilizi g low-temperature steam, Energy Procedia 63 (2014) 2249–2254.
[18] K. Kim, et al., Moving bed adsorption process with internal heat integration for carbon dioxide capture, Int. J. Greenhouse Gas Control 17 (2013) 13–24.
[19] J.-Y. Kim, et al., Continuous testing of silica-PEI adsorbents in a lab.-scale twin bubbling fluidized-bed system, Int. J. Greenhouse Gas Control 82 (2019) 184–191.
[20] C.-K. Yi, et al., Continuous operation of the potassium-based dry sorbent CO2 capture process with two fluidized-bed reactors, Int. J. Greenhouse Gas Control 1 (1) (2007) 31–36.
[21] C.A. Grande, et al., Electric swing adsorption as emerging CO2 capture technique, Energy Procedia 1 (1) (2009) 1219–1225.
[22] C.A. Grande, A.E. Rodrigues, Electric swing adsorption for CO2 removal from flue gases, Int. J. Greenhouse Gas Control 2 (2) (2008) 194–202.
[23] L. Riboldi, O. Bolland, Evaluating pressure swing adsorption as a CO2 separation technique in coal-fired power plants, Int. J. Greenhouse Gas Control 39 (2015) 1–16.
[24] K. Warmuzinski, M. Tanczyk, M. Jaschik, Experimental study on the capture of CO2 from flue gas using adsorption combined with membrane separation, Int. J. Greenhouse Gas Control 37 (2015) 182–190.
[25] M.G. Plaza, F. Rubiera, C. Pevida, Evaluating the feasibility of a TSA process based on steam stripping in combination with structured carbon adsorbents to capture CO2 from a coal power plant, Energy Fuels 31 (9) (2017) 9760–9775.
[26] R.P. Lively, et al., Hollow fiber adsorbents for CO2 removal from flue gas, Ind. Eng. Chem. Res. 48 (15) (2009) 7314–7324.
[27] Q. Zhao, et al., CO2 capture using a novel hybrid monolith (H-ZSM5/activated carbon) as adsorbent by combined vacuum and electric swing adsorption (VESA), Chem. Eng. J. 358 (2019) 707–717.
[28] N. Querejeta, et al., Carbon monoliths in adsorption-based post-combustion CO2 capture, Energy Procedia 114 (2017) 2341–2352.
[29] F. Dietrich, et al., Experimental study of the adsorber performance in a multi-stage fluidized bed system for continuous CO2 capture by means of temperature swing adsorption, Fuel Process. Technol. 173 (2018) 103–111.
[30] T. Proell, et al., Introduction and evaluation of a double loop staged fluidized bed system for post-combustion CO2 capture using solid sorbents in a continuous temperature swing adsorption process, Chem. Eng. Sci. 141 (2016) 166–174.
[31] S. Roy, C.R. Mohanty, B.C. Meikap, Multistage fluidized bed reactor performance characterization for adsorption of carbon dioxide, Ind. Eng. Chem. Res. 48 (23) (2009) 10718–10727.
[32] A. Zaabout, et al., Thermodynamic assessment of the swing adsorption reactor cluster (SARC) concept for post-combustion CO2 capture, Int. J. Greenhouse Gas Control 60 (2017) 74–92.
[33] S. Cloete, et al., The effect of sorbent regeneration enthalpy on the performance of the novel Swing Adsorption Reactor Cluster (SARC) for post-combustion CO2 capture, Chem. Eng. J. (2018).
[34] S. Cloete, et al., The swing adsorption reactor cluster for post-combustion CO2 capture from cement plants, J. Clean. Prod. 223 (2019) 692–703.
[35] C. Dhoke, et al., The swing adsorption reactor cluster (SARC) for post combustion CO2 capture: experimental proof-of-principle, Chem. Eng. J. (2018).
[36] W. Choi, et al., Epoxide-functionalization of polyethyleneimine for synthesis of stable carbon dioxide adsorbent in temperature swing adsorption, Nat. Commun. 7 (2016) 12640.
[37] I. Luz, M. Soukri, M. Lail, Confining metal-organic framework nanocrystals within mesoporous materials: a general approach via “solid-state” synthesis, Chem. Mater. 29 (22) (2017) 9628–9638.
[38] I. Luz, M. Soukri, M. Lail, Flying MOFs: polyamine-containing fluidized MOF/SiO2 hybrid materials for CO2 capture from post-combustion flue gas, Chem. Sci. 9 (20) (2018) 4589–4599.